



This is a repository copy of *Meta-atom based two-sphere Newton's cradle*.

White Rose Research Online URL for this paper:

<https://eprints.whiterose.ac.uk/id/eprint/232645/>

Version: Published Version

---

**Article:**

Pope, S.A. orcid.org/0000-0001-8130-4222 and Wright, O.B. orcid.org/0000-0003-3035-0901 (2025) Meta-atom based two-sphere Newton's cradle. *Physical Review E*, 112 (3). 035506. ISSN: 2470-0045

<https://doi.org/10.1103/2whk-jc4b>

---

**Reuse**

This article is distributed under the terms of the Creative Commons Attribution (CC BY) licence. This licence allows you to distribute, remix, tweak, and build upon the work, even commercially, as long as you credit the authors for the original work. More information and the full terms of the licence here:


<https://creativecommons.org/licenses/>

**Takedown**

If you consider content in White Rose Research Online to be in breach of UK law, please notify us by emailing [eprints@whiterose.ac.uk](mailto:eprints@whiterose.ac.uk) including the URL of the record and the reason for the withdrawal request.



[eprints@whiterose.ac.uk](mailto:eprints@whiterose.ac.uk)  
<https://eprints.whiterose.ac.uk/>

**Meta-atom based two-sphere Newton's cradle**Simon A. Pope <sup>\*</sup>*Department of Automatic Control and Systems Engineering, University of Sheffield, Mappin Street, Sheffield S1 3JD, United Kingdom*Oliver B. Wright *Hokkaido University, Sapporo 060-0808, Japan**and Graduate School of Engineering, The University of Osaka, 2-1 Yamadaoka, Suita, Osaka 565-0871, Japan*

(Received 25 April 2025; accepted 18 August 2025; published 25 September 2025; corrected 2 October 2025)

Locally resonant metamaterials are among the most studied types of elastic and acoustic metamaterials, with significant research focused on wave propagation in a periodic array of “meta-atoms.” Here we investigate the collision dynamics of two identical pendulum-suspended mass-in-mass resonators, essentially a two-sphere Newton's cradle, emphasizing the readily realizable scenario where the internal resonator frequency is much greater than the pendulum frequency. We first show that the dynamics of a collision can be described using effective parameters, similar to how previous metamaterials research has characterized wave propagation through effective material parameters. Nonconventional collision dynamics—observed in two colliding mass-in-mass systems where one is initially at rest—include behaviors such as the moving sphere rebounding as if from a fixed wall while the other remains essentially stationary, the spheres coupling and moving forward in near-unison, and the spheres recoiling in opposite directions. These responses can be achieved by tuning the effective parameters. We demonstrate that these parameters can take on values that differ significantly from those in a conventional Newton's cradle. Additionally, we investigate multiple collisions of the two spheres, revealing complex dynamics. This work paves the way for the development and study of new “collision-based metamaterial” structures.

DOI: [10.1103/2whk-jc4b](https://doi.org/10.1103/2whk-jc4b)**I. INTRODUCTION**

Metamaterials are engineered structures that exhibit effective parameters not typically found in conventional materials [1]. Some of the most widely discussed parameters are those that affect wave propagation within the bulk of the metamaterial, such as the effective density and modulus. Methods for designing such metamaterials, in which one or more of these effective parameters is negative for a desired frequency band, are of particular interest [2], since negative effective values fundamentally modify behavior compared to conventional materials and enable novel applications [3,4].

Wave propagation in elastic metamaterials is typically considered in the context of an effective continuum that is permanently elastically connected. A class of widely studied structures corresponds to mass-in-mass locally resonant metamaterials [2,5,6], where a lattice of connected masses each has a local resonator attached. In most formulations of mass-in-mass systems, the resulting dynamics are described by a frequency-dependent effective mass. A sufficiently strong

resonance creates a frequency band in which the effective mass is negative, resulting in a complex modulus that attenuates wave propagation within this band. Some research has focused on wave propagation in granular metamaterials, composed of closely packed discrete entities [7]. The contact between these entities is inherently nonlinear, with individual entities resisting compression but separating under tension. Some studies have concentrated on precompressed systems that do not separate under tension forces smaller than the precompressing force. This includes a one-dimensional array of beads with local “ring” resonators [8], which showed a transmission bandgap typical of single-negative metamaterials. The effect of resonant inclusions on the transmission, reflection, and localization of energy has been investigated for a single bead, and subsequently extended to two and three beads in a sequence initially in contact [9].

Other related work on granular metamaterials has examined their response as the ratio of resonator mass to transmission medium mass tends to zero [10]. Separate work has also explored the generation and identification of stationary and traveling waves in such structures [11–15]. A “woodpile” metamaterial design has also been investigated [16], where the meta-atoms are not permanently elastically connected but stacked so that they can separate and collide under specific conditions. One common feature across this previous work is the focus on multiple collisions and their associated wave propagation. However, the fundamental processes involved in individual collisions in such metamaterials and their effect

<sup>\*</sup>Contact author: [s.a.pope@sheffield.ac.uk](mailto:s.a.pope@sheffield.ac.uk)

Published by the American Physical Society under the terms of the [Creative Commons Attribution 4.0 International](https://creativecommons.org/licenses/by/4.0/) license. Further distribution of this work must maintain attribution to the author(s) and the published article's title, journal citation, and DOI.

on the overall dynamics have not been extensively studied or compared to conventional collision dynamics.

The best-known demonstration of collisions between conventional entities is Newton's cradle. Although commonly seen as an executive toy, it still holds significance from a research perspective. Its relatively simple setup can be modified to test collisions between "nonstandard" entities. An interesting example involves a modified Newton's cradle where the spheres are coated in fluid, creating a "Stokes cradle" [17,18]. In a conventional three-sphere Newton's cradle with elastic collisions, releasing one sphere causes the opposite sphere to swing away. However, in a Stokes cradle with liquid-coated spheres, four responses can occur depending on Stokes number: the standard response (last sphere moves, first two remain), all three cluster, the last two cluster and move together, or all three separate. These outcomes depend on the Stokes number and liquid coating thickness.

In this paper, we use a model of a frictionless two-sphere Newton's cradle, modified so that the colliding entities are hollow mass-in-mass resonators. We investigate the effect of the local resonators on the fundamental properties of individual collisions between the outer spherical shells in a readily realizable case where the internal resonator frequency is significantly greater than the pendulum frequency. We show that the calculated velocities at the moment of separation can be expressed in a form equivalent to conventional sphere collisions. From this, we derive effective coefficients of restitution and motion using an approach similar to those typically applied in continuum metamaterials. However, unlike previous approaches, we determine these effective parameters in the time domain, as they are strictly defined only at the moment the shells separate at the end of a collision. These effective parameters can take nonconventional values, including negative ones. We show that by varying the ratio of the resonator frequency to the fundamental "compression frequency" of the colliding outer masses and the energy stored in the local resonators, it is possible to achieve separation velocities that do not comply with the conventional conservation of momentum for the outer masses. We also elucidate the possible temporal evolutions of this two-sphere cradle.

## II. THEORY AND MODELING

### A. Basic equations of motion

The colliding spheres are assumed to be two identical, suspended, frictionless mass-in-mass resonators, as shown in Fig. 1(a), which can swing in a single plane, resembling a two-sphere Newton's cradle. In a practical Newton's cradle configuration, a single suspension wire for each mass is replaced by two wires to ensure such motion. The spheres can be visualized as spherical shells, inside which a linear one-dimensional mass-spring resonator is attached. We refer to the shell on the left, along with its internal resonator, as mass-in-mass system 1, and the equivalent structure on the right as mass-in-mass system 2. The angle  $\theta_i$  ( $i = 1, 2$ ) is the angular displacement of the shell of system  $i$ . The spherical shells are assumed to be suspended by identical wires of negligible mass attached to a fixed point above. This provides an external gravitational potential that acts to return both shells to

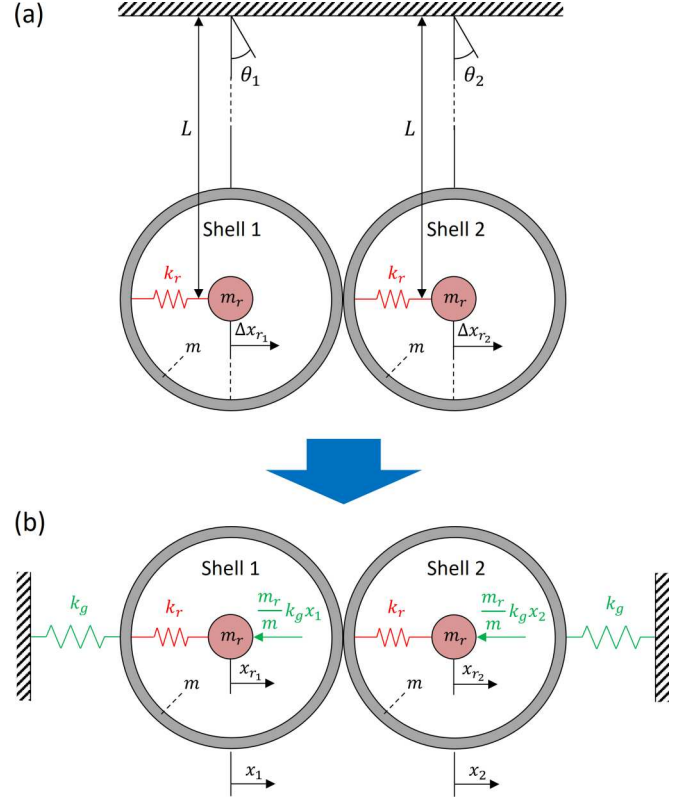


FIG. 1. (a) The two-sphere mass-in-mass colliding pendulum system (a modified Newton's cradle), along with (b) the equivalent approximate pure mass-and-spring model applicable for small displacements and stiff spherical shells, which exhibits one-dimensional motion. The chosen model for the dynamics during a collision, which depends on the collision stiffness  $k_c$  in a linear approximation, is not shown. In this paper, we assume that the right-hand shell and its internal mass are in their equilibrium positions before the first collision.

their undisturbed positions, defined by the condition  $\theta_{1,2} = 0$ . In these positions the external shells are positioned so that they are just touching, with their gravitational potential energy at its minimum. The resonator masses are assumed to be spherical (although this is not a required assumption) and, for simplicity, are assumed to be in their central positions when in equilibrium. They are constrained to move perpendicular to the supporting wire, and  $\Delta x_{ri}$  is the component of the extension of a spring connected to its internal mass. The mass of the springs is assumed to be negligible compared to the other masses.

To simplify the analysis of this colliding mass-in-mass system, a one-dimensional motion approximation is applied. This is illustrated in Fig. 1(b), where  $x_i$  ( $x_{ri}$ ) represent the relative displacements of the outer spherical shells (internal resonators) from their equilibrium positions. As demonstrated in the Supplemental Material [19], and under the assumption of small displacements, the effect of gravity on the angular motion of the spherical shells can be approximated by modeling the wires as linear springs, with a spring constant given by  $k_g = mg/L$ . Here,  $m$  represents the mass of the spherical shells,  $g$  is the acceleration due to gravity, and  $L$  is the

effective length of the pendulums, measured from the support to the center of the shells. This represents the gravitational potential relative to the undisturbed position of each shell (which is taken as zero for an undisturbed shell). In Fig. 1(b), gravitational effects are indicated in green, whereas the effect of gravity on an internal mass is represented as an external force, given by  $(m_r/m)k_g x_{r_i}$ , since it cannot be depicted solely by a spring attached to the internal mass. The resulting resonance frequency is given by  $\omega_g = \sqrt{k_g/m} = \sqrt{g/L}$ . The mass and spring constant of the internal linear resonators are defined as  $m_r$  and  $k_r$ , respectively, with the associated angular resonance frequency  $\omega_r = \sqrt{k_r/m_r}$ . The motion is assumed to be lossless. The present work does not focus on exploring various resonator designs that could physically realize the desired dynamics. Instead, we use the simple representative example shown in Fig. 1(b), featuring spherical masses, to investigate the fundamental dynamics of such systems.

The equations of motion for the two shells with internal resonators, which oscillate freely in a one-dimensional potential field until they come into contact with one another, can be modeled as a piecewise system. A similar approach has previously been used to model the conventional Newton's cradle [20]. To ensure that the contact force only acts under compression (i.e., that no forces act to resist tension), we use Eqs. (1) to describe the motion when the shells are in contact for  $x_2 - x_1 \leq 0$  and Eqs. (2) (describing pendulum dynamics) when the shells are not in contact:

when  $x_2 - x_1 \leq 0$ ,

$$m\ddot{x}_1 = k_c(x_2 - x_1) - k_g x_1 + k_r(x_{r_1} - x_1), \quad (1a)$$

$$m_r\ddot{x}_{r_1} = -\frac{m_r}{m}k_g x_1 + k_r(x_1 - x_{r_1}), \quad (1b)$$

$$m\ddot{x}_2 = -k_c(x_2 - x_1) - k_g x_2 + k_r(x_{r_2} - x_2), \quad (1c)$$

$$m_r\ddot{x}_{r_2} = -\frac{m_r}{m}k_g x_2 + k_r(x_2 - x_{r_2}), \quad (1d)$$

otherwise,

$$m\ddot{x}_1 = -k_g x_1 + k_r(x_{r_1} - x_1), \quad (2a)$$

$$m_r\ddot{x}_{r_1} = -\frac{m_r}{m}k_g x_1 + k_r(x_1 - x_{r_1}), \quad (2b)$$

$$m\ddot{x}_2 = -k_g x_2 + k_r(x_{r_2} - x_2), \quad (2c)$$

$$m_r\ddot{x}_{r_2} = -\frac{m_r}{m}k_g x_2 + k_r(x_2 - x_{r_2}). \quad (2d)$$

During contact, the force between the spherical shells is assumed to be compressive. Contact forces result from the relatively small indentation of the shells in the region around the contact point, and for purposes of approximation we ignore in Eqs. (1) the Hertzian-contact nonlinearity and assume this compressive force to be linear in indentation, as was done previously for the case of contacting spherical shells [21–23]. The contact stiffness of the shell is defined as  $k_c = O(Eh^2/2R)$ , where  $E$  is the Young's modulus of the shell material,  $h$  is the thickness of the shell, and  $R$  is the shell outer radius. In contrast, the indentation of solid spheres requires precise treatment using (nonlinear) Hertzian theory [24], combined with the theory of shell deformation. We also define a

characteristic compression angular frequency  $\omega_c = \sqrt{2k_c/m}$ , which is useful in the elucidation of the contact dynamics.

Equations (1) represent a set of unforced equations governing the contact dynamics. During a collision, the initial conditions of Eqs. (1) are determined by the pendulum dynamics given by Eqs. (2) at the time of contact  $t_c$ , defined by  $(x_2 - x_1)_{t_c} = 0$ . For simplicity of the analysis throughout this paper, the state of the shells at the start of a collision are taken as those of a conventional Newton's cradle; the first shell moves and collides with the second shell, which, along with its internal resonator, is initially stationary at the equilibrium position (i.e., having zero potential and kinetic energy). This gives  $x_{1,t_c} = x_{2,t_c} = \dot{x}_{2,t_c} = 0$  and  $\dot{x}_{1,t_c} \neq 0$ . The contact period is defined as the period  $[t_c, t_s]$  between the shells making contact at time  $t_c$  and then separating at time  $t_s$ , that is, the period during which  $(x_2 - x_1) \leq 0$ . The state of the system at the end of the contact period (i.e., at  $t_s$ ) then defines the initial conditions for the pendulum dynamics governing the motion after separation.

## B. Derivation of the effective parameters and determination of the postcollision velocities

The coefficient of restitution (CR) is one of the most commonly used quantities used to describe the collision between two bodies. It is usually defined in terms of the ratio of the relative separation to relative collision velocity:

$$\text{CR} = (\dot{x}_2 - \dot{x}_1)_{t_s} / (\dot{x}_1 - \dot{x}_2)_{t_c}. \quad (3)$$

The postcollision velocities for a simple collision between two hard, solid spheres, such as in a basic model of a conventional Newton's cradle, where the second sphere is initially at rest ( $\dot{x}_{2,t_c} = 0$ ) and where momentum is conserved and assumed to be transferred instantaneously, can be written in the following form:

$$\dot{x}_{1,t_s} = \frac{m_1 - m_2 \text{CR}}{m_1 + m_2} \dot{x}_{1,t_c}, \quad (4a)$$

$$\dot{x}_{2,t_s} = \frac{m_1 + m_1 \text{CR}}{m_1 + m_2} \dot{x}_{1,t_c}. \quad (4b)$$

For identical spheres this reduces to

$$\dot{x}_{1,t_s} = \frac{1}{2}(1 - \text{CR})\dot{x}_{1,t_c}, \quad (5a)$$

$$\dot{x}_{2,t_s} = \frac{1}{2}(1 + \text{CR})\dot{x}_{1,t_c}. \quad (5b)$$

The coefficient of restitution CR represents how well energy is conserved in the collision.  $\text{CR} = 1$  for a conventional two-sphere Newton's cradle with linear lossless compression during contact, which represents a perfectly elastic collision. The “1” in Eqs. (5) arises owing to the conservation of momentum: addition of Eqs. (5a) and (5b) to eliminate CR leads to the momentum conservation equation  $\dot{x}_{1,t_s} = \dot{x}_{1,t_c} + \dot{x}_{2,t_s}$  for identical spheres. Using this understanding, we can write a more general form of Eqs. (5) as follows:

$$\dot{x}_{1,t_s} = \frac{1}{2}(\text{CM}_e - \text{CR}_e)\dot{x}_{1,t_c}, \quad (6a)$$

$$\dot{x}_{2,t_s} = \frac{1}{2}(\text{CM}_e + \text{CR}_e)\dot{x}_{1,t_c}. \quad (6b)$$

Here we define an effective coefficient of restitution in the same manner as in the conventional sense:

$$\text{CR}_e = \frac{\dot{x}_{2,t_s} - \dot{x}_{1,t_s}}{\dot{x}_{1,t_c}}, \quad (7a)$$

$$\text{CM}_e = \frac{\dot{x}_{1,t_s} + \dot{x}_{2,t_s}}{\dot{x}_{1,t_c}}. \quad (7b)$$

We also define an effective “coefficient of motion” term in Eqs. (7b) as the ratio of the momentum after to that before the collision of two identical spheres. When momentum is conserved,  $\text{CM}_e = 1$ . We can now use this more general definition to represent the collision of mass-in-mass spheres, and understand how the internal resonators influence the resulting postcollision motion. We refer to these variables as “effective” coefficients, since we will show that they serve to characterize

the dynamics of the two colliding locally resonant spheres, and are a function of the internal resonator parameters. This “effective systems approach” is analogous to that previously used to describe wave propagation in mass-in-mass continuum metamaterials.

To determine the effective coefficients of motion and restitution for the collision of such mass-in-mass entities, one needs to consider the velocities of both the spherical shells and the inner masses at the moment of separation. By taking into account the initial conditions at the moment of collision and making use of Eqs. (1) in the Laplace domain, one can eliminate  $x_{r1}$  and  $x_{r2}$  to obtain equations for  $\dot{x}_{2,t_s} - \dot{x}_{1,t_s}$  and  $\dot{x}_{2,t_s} + \dot{x}_{1,t_s}$  for purposes of substitution into Eqs. (7a) and (7b), respectively, under the additional assumption of stiff shells, i.e.,  $\omega_g \ll \omega_c$  (see the Supplemental Material [19] and estimates in the main text below):

$$\text{CR}_e = -\mathcal{L}^{-1} \left( \frac{\hat{m}_{e,s} s}{\hat{m}_e s^2 + \omega_c^2} \left( \frac{x_{r1,t_c}}{\dot{x}_{1,t_c}} s + \frac{\dot{x}_{r1,t_c}}{\dot{x}_{1,t_c}} \right) + \frac{s}{\hat{m}_e s^2 + \omega_c^2} \right) \Big|_{t=t_s}, \quad (8a)$$

$$\text{CM}_e = \mathcal{L}^{-1} \left( \frac{\hat{m}_{e,s}}{\hat{m}_e s} \left( s \frac{x_{r1,t_c}}{\dot{x}_{1,t_c}} + \frac{\dot{x}_{r1,t_c}}{\dot{x}_{1,t_c}} \right) + \frac{1}{\hat{m}_e s} \right) \Big|_{t=t_s}, \quad (8b)$$

where

$$\hat{m}_e = 1 + \frac{m_r}{m} \frac{\omega_r^2}{s^2 + \omega_r^2} = 1 + \hat{m}_{e,s}. \quad (9)$$

These equations describe the effective coefficients of restitution and motion, respectively, where  $\mathcal{L}^{-1}$  denotes the inverse Laplace transform. For ease of analysis, the time domain has been shifted such that  $t_c = 0$ . In this paper, we focus on the case in which the local resonant frequency is commensurate with the compression frequency, i.e.,  $\omega_r \sim \omega_c$ , as this condition represents the one most practically accessible and where the effect of the internal resonators becomes most pronounced.

The result is that the effective coefficient of restitution is a function of two angular frequencies resulting from (1) the interaction during contact of the spherical shells, characterized by  $\omega_c = \sqrt{2k_c/m}$ , and (2) the local-resonance dynamics, characterized by  $\omega_r = \sqrt{k_r/m_r}$ , whereas the effective coefficient of motion is a function of  $\omega_r$  only. Both effective coefficients are a function of the resonator conditions at the moment of collision.

It is pertinent at this point to justify the above assumptions for a practical situation by giving order of magnitude estimates of a possible configuration for experimental realization of a two-sphere mass-in-mass Newton’s cradle. This also helps to visualize an actual future experimental configuration. Reasonable values for a possible implementation are as follows: steel shells of outer radius  $R = 10$  mm and wall thickness 1 mm, and inner tungsten spheres of radius 5 mm, leading to masses  $m = 8.9$  g,  $m_r = 10.1$  g, gravitational spring constant  $k_g = 0.87$  N/m, contact stiffness  $k \approx 9.5 \times 10^6$  N/m, making use of the Young’s modulus of steel  $E = 190$  GPa, density of steel  $7850$  kg m<sup>−3</sup>, density of tungsten  $19250$  kg m<sup>−3</sup> and wire length  $L = 100$  mm; one can, for example, choose the inner-spring constant value of

$k_r = 2 \times 10^6$  N/m, in line with commercially available stiff coil springs of length 5 mm. The resulting resonant frequencies correspond to compression frequency  $\omega_c/2\pi = 7340$  Hz, local-resonator frequency  $\omega_r/2\pi = 2240$  Hz and pendulum-resonance frequency  $\omega_g/2\pi = 1.6$  Hz. Clearly, this justifies the stiff shell approximation,  $\omega_g \ll \omega_c$ , and the assumption that  $\omega_r \sim \omega_c$ , both of which will be applied in the subsequent analysis. The equivalent conditions for the spring stiffness are  $\sqrt{k} \sim \sqrt{mk_r/2m_r}$ , and  $\sqrt{k_g} \ll \sqrt{2k}$ . This ensures that the local resonator frequency is significantly lower than the resonant frequency of acoustic waves within the sphere, maintaining the validity of the lumped element approximation. Furthermore, we neglect the effect of acoustic waves generated in the wire by the high-frequency internal oscillator.

By increasing the shell radius  $R$  while maintaining its thickness at  $0.1R$ , the compression frequency is reduced—enabling a more practical physical implementation using resonator springs with lower stiffness and greater length. The compression frequency can also be decreased by selecting a softer shell material (e.g., acrylic). We assume that the characteristic angular frequencies  $\omega_g$ ,  $\omega_c$ , and  $\omega_r$  are all well removed from any natural resonant frequencies of the individual shells (such as that of the  $n = 2$  flexural mode).

We carried out simulations with softer shells (resulting in longer contact times) and material losses (nonelastic collisions) to confirm that the subsequent analysis remains valid unless the choice of elastic parameters violates the inequalities involving the characteristic frequencies.

For practical implementation, the internal stiffness could be achieved with a commercially available coil spring, as previously mentioned. Alternatively, leaf springs could provide sufficient stiffness while providing directional constraint. Further constraint of the internal mass’s motion along the line of collision could be implemented using a drilled mass sliding along a guiding rod attached to the shell’s interior.



The initial conditions of the internal mass in shell 1 (e.g., its potential and kinetic energy) could be set manually by pulling a rod extending from a hole in the shell opposite to the collision surface—and/or through more complex electromechanical methods, such as electronically releasing a preloaded resonator spring just before a collision.

Importantly, the derivations and analysis presented are valid for collisions occurring normal (i.e., perpendicular) to the surface of any body, provided the underlying assumptions hold. For instance, the collision of two trolleys containing internal resonators on a track curved in the vertical direction could serve as an alternative experimental validation of the principles discussed.

The effective coefficients as described above are written as a function of the same effective mass that has been the focus of previous work on mass-in-mass continuum metamaterials [5]. However, the effective coefficients that we are focusing on here are defined in the time domain, as opposed to the frequency domain usually considered in metamaterials research. The reason for using the time domain in this case is that the frequency domain is less intuitive, as the effective parameters are defined at a single moment in time, i.e., when the shells separate. These parameters are considered effective because they encapsulate both the effects of collision dynamics and the influence of the resonators' motion on the overall movement of the spherical shells. Under our approximations, the duration of the collisions is governed by unforced dynamics, determined solely by the individual mass-in-mass system parameters and the associated initial conditions. The final state of the impact occurs when the two entities separate, at which point the governing dynamics change. Use of the time domain rather than the frequency domain makes the analysis slightly less straightforward owing to the dependence of Eqs. (8a) and (8b) on the moment of separation  $t_s$ . The moment of separation also depends on the interaction during contact of the resonances at  $\omega_c$  and  $\omega_r$  and on the resonator initial conditions, and is defined as the moment corresponding to the first instance when  $x_2 - x_1 = 0$  after time  $t_c$ . As a consequence of this complexity, a simple analytical solution to the effective coefficients does not exist, and numerical solutions are required.

### C. Derivation of effective parameters for general motion in the external potential postcollision

The instantaneous velocities of the two spherical shells,  $\dot{x}_{1,t_s}$  and  $\dot{x}_{2,t_s}$ , at the moment of separation do not completely define the motion after separation. This can be seen by solving Eqs. (2) for  $\dot{x}_1$  and  $\dot{x}_2$  at  $t_s$  and using initial conditions for the shell and internal resonator motion at the moment of separation. Since the compression angular frequency  $\omega_c$  is, in practice, that appropriate to stiff colliding shells (i.e.,  $\omega_g \ll \omega_c$ ), and, owing to the relatively weak pendulum spring stiffnesses in a Newton's cradle setup,  $\omega_g \ll \omega_r$ . The velocity of a sphere after separation can be derived as follows (see the Supplemental Material [19] for the full derivation):

$$\begin{aligned} \dot{x}_i = & -\frac{m\dot{x}_{i,t_s} + m_r\dot{x}_{r_i,t_s}}{m + m_r} \omega_g \sin(\omega_g t_{s^+}) \\ & + \frac{m\dot{x}_{i,t_s} + m_r\dot{x}_{r_i,t_s}}{m + m_r} \cos(\omega_g t_{s^+}) \end{aligned}$$

$$\begin{aligned} & -m_r \frac{\dot{x}_{i,t_s} - \dot{x}_{r_i,t_s}}{m + m_r} \sqrt{\frac{m + m_r}{m}} \omega_r \sin\left(\sqrt{\frac{m + m_r}{m}} \omega_r t_{s^+}\right) \\ & + m_r \frac{\dot{x}_{i,t_s} - \dot{x}_{r_i,t_s}}{m + m_r} \cos\left(\sqrt{\frac{m + m_r}{m}} \omega_r t_{s^+}\right), \end{aligned} \quad (10)$$

where  $t_{s^+}$  is the time after separation, namely  $t_{s^+} = t - t_s$ . The postcollision velocity is therefore a sum of oscillatory terms at two angular frequencies. One of these is the pendulum angular frequency  $\omega_g$  and the other the much higher mass-weighted local-resonance angular frequency  $\omega_r \sqrt{(m + m_r)/m}$ . Assuming that the magnitude of the higher frequency oscillation is sufficiently small so that the shells do not collide again shortly after they separate, the general motion in the external potential is determined by the terms involving  $\omega_g$  in Eqs. (10). This assumption is usually satisfied when  $\omega_g \ll \omega_r$ , since the displacement amplitude of the mass-weighted local resonator is proportional to  $1/\omega_r$ . Under such conditions, the total instantaneous postcollision velocities defined in Eqs. (10) can be simplified to the following form by setting  $t_{s^+} = 0$ :

$$\begin{aligned} \dot{x}_{i,t_s} = & \frac{m\dot{x}_{i,t_s} + m_r\dot{x}_{r_i,t_s}}{m + m_r} + m_r \frac{\dot{x}_{i,t_s} - \dot{x}_{r_i,t_s}}{m + m_r} \\ = & \dot{x}_{i,a} + \dot{x}_{i,r}. \end{aligned} \quad (11)$$

The first term is the contribution from the motion in the external potential and the second is a contribution from the resonator causing the sphere to oscillate with respect to the motion in the general external potential.

We can therefore define two sets of effective collision parameters. One set describes the total instantaneous velocity of the sphere at the moment of separation, as outlined by Eqs. (7a) and (7b). The other set characterizes the instantaneous effect of the collision on the general motion in the external potential after the collision, defined by the initial velocities,  $\dot{x}_{i,a}$ , of the oscillatory motion associated with the resonant frequency of the external potential. The effective coefficient of restitution for the general motion in the external potential can be defined in the same manner as the conventional coefficient of restitution, i.e.,  $\text{CR}_a = (\dot{x}_{2,a} - \dot{x}_{1,a})/(\dot{x}_{1,t_c} - \dot{x}_{2,t_c})$ . Taking the same initial conditions at the point of contact, namely  $\dot{x}_{2,t_c} = 0$ , and substituting for  $\dot{x}_{1,a}$  and  $\dot{x}_{2,a}$  from Eqs. (11), we obtain

$$\begin{aligned} \text{CR}_a = & \frac{1}{m + m_r} \frac{m(\dot{x}_{2,t_s} - \dot{x}_{1,t_s}) + m_r(\dot{x}_{r2,t_s} - \dot{x}_{r1,t_s})}{\dot{x}_{1,t_c}}, \\ = & \frac{1}{m + m_r} (m\text{CR}_e + m_r\text{CR}_r), \end{aligned} \quad (12a)$$

$$\begin{aligned} \text{CM}_a = & \frac{1}{m + m_r} \frac{m(\dot{x}_{2,t_s} + \dot{x}_{1,t_s}) + m_r(\dot{x}_{r2,t_s} + \dot{x}_{r1,t_s})}{\dot{x}_{1,t_c}}, \\ = & \frac{1}{m + m_r} (m\text{CM}_e + m_r\text{CM}_r). \end{aligned} \quad (12b)$$

The effective coefficient of restitution for the general motion in the external potential is thus given by a mass-weighted sum of two effective coefficients of restitution: the instantaneous effective coefficient of restitution and a new effective coefficient of restitution arising from the resonators. An

effective coefficient of motion  $CM_a$  for the general motion can be derived in a comparable manner, leading to Eqs. (12b). Similarly, for the velocities,

$$\dot{x}_{1,a} = \frac{1}{2}(CM_a - CR_a)\dot{x}_{1,t_c}, \quad (13a)$$

$$\dot{x}_{2,a} = \frac{1}{2}(CM_a + CR_a)\dot{x}_{1,t_c}. \quad (13b)$$

$$CR_a = \frac{m}{m + m_r} \left( CR_e + (\hat{m}_{e,s}(t) * CR_e(t))|_{t=t_s} - \omega_r^2 \left( \frac{d^2 \hat{m}_{e,s}(t)}{dt^2} \frac{x_{r1,t_c}}{\dot{x}_{1,t_c}} + \frac{d \hat{m}_{e,s}(t)}{dt} \frac{\dot{x}_{r1,t_c}}{\dot{x}_{1,t_c}} \right) \Big|_{t=t_s} \right), \quad (14a)$$

$$CM_a = \frac{m}{m + m_r} \left( 1 + \frac{m_r}{m} \frac{\dot{x}_{r,t_c}}{\dot{x}_{1,t_c}} \right). \quad (14b)$$

These equations are written in the time domain, where "(t)" denotes the time domain form of the equations for the effective mass and coefficient of restitution of the instantaneous velocity prior to their calculation at the moment of separation.

### III. RESULTS AND DISCUSSION

#### A. Parametric studies of the dynamics of a particular system

To aid analysis and without significant loss of generality, we consider the particular case where the resonator mass is equal to the spherical-shell mass, i.e.,  $m_r = m$ . We define  $\Omega = \omega_r/\omega_c$ , so for a constant  $\omega_c$ , determined by the shell material, one can consider variations in  $\Omega$  for the case of a constant resonator mass  $m_r$  as equivalent to variations in the resonator spring constant  $k_r$ . In this paper we investigate the range  $0.03 \lesssim \Omega \lesssim 30$ . All results for the following parametric studies are obtained through numerical analysis conducted using MathWorks MATLAB.

Conditions for a stiff sphere are implemented using a steel shell with a radius of  $R = 10$  mm and shell thickness  $0.1R$ , leading to  $\omega_c/\omega_g = 4.7 \times 10^4$ . The initial conditions of the internal resonator of the (left-hand) mass-in-mass system 1 at the moment of collision are described in terms of  $E_n$ , the total energy (including both kinetic and potential energy) of the resonator relative to the kinetic energy of an equivalent nonresonant sphere of mass  $m$ , and  $\phi_{r1,t_c}$ , the phase of the internal resonant mass relative to its undisturbed location (plotted on the vertical axis of each panel). Further,  $x_{r1,t_c}/\dot{x}_{1,t_c} = \sqrt{E_n}/\omega_r^2 \sin \phi_{r1,t_c}$  and  $\dot{x}_{r1,t_c}/\dot{x}_{1,t_c} = \sqrt{E_n} \cos \phi_{r1,t_c}$ . A phase of 0 or  $\pi$  corresponds to no potential energy stored in the resonator, and a phase of  $\pi/2$  or  $3\pi/2$  corresponds to no kinetic energy stored in the resonator.

Figure 2 shows density plots where color represents the effective coefficients of motion  $CM_a$  (left panels) and restitution  $CR_a$  (right panels). The vertical axes show the phase  $\phi_{r1,t_c}$  of the resonator 1 at the moment of collision, and the horizontal axes represent the normalized frequency ratio  $\Omega = \omega_r/\omega_c$ . The total resonator energy increases from top to bottom in each column, with its value labeled in each panel. Green represents zero on the color scale, with positive values indicated by warmer colors and negative values by cooler colors.

Figure 3 shows a "phase diagram" (color scale) for the two colliding mass-in-mass systems as a function of resonator

To determine the additional effective collision parameters  $CR_r$  and  $CM_r$ , the velocity of the resonator masses at the moment of separation needs to be included. The Supplemental Material contains the derivation of these terms and the effective coefficients for general velocities [19]. The resulting effective coefficient of restitution and motion in this case can be expressed in the form

parameters and initial conditions, with the same horizontal and vertical axes as in Fig. 2. The plots are generated from the initial velocities of each spherical shell in the external potential after impact. These are included as density plots in the Supplemental Material [19]. Each color represents a different dynamic response, which can be interpreted in terms of the effective collision parameters, as follows:

Rigid wall:

$$(-0.1 < \dot{x}_{1,a}) \text{ \& } (0 \leq \dot{x}_{2,a} < 0.1).$$

Shell 1 rebounds in the opposite direction to its precollision velocity and shell 2 is stationary.

Coupling:

$$(0.1 < \dot{x}_{1,a}) \text{ \& } (0.1 < \dot{x}_{2,a}) \text{ \& } (1 \leq |\dot{x}_{2,a}|/|\dot{x}_{1,a}| \leq 1.1).$$

Shells 1 and 2 have equal velocities in the same direction as the initial momentum of shell 1.

Same direction:

$$(\dot{x}_{1,a} > 0) \text{ \& } (\dot{x}_{2,a} > 0).$$

Shells 1 and 2 have velocities in the same direction as the initial momentum of shell 1.

Recoiling:

$$(\dot{x}_{1,a} < -0.1) \text{ \& } (\dot{x}_{2,a} > 0.1) \text{ \& } (0.9 \leq |\dot{x}_{2,a}|/|\dot{x}_{1,a}| \leq 1.1).$$

Shells 1 and 2 have equal and opposite velocities.

Opposite velocities:

$$(\dot{x}_{1,a} < 0) \text{ \& } (\dot{x}_{2,a} > 0).$$

Shells 1 and 2 have opposite velocities.

Stationary shell 1 (smaller  $\dot{x}_{2,a}$ ):

$$(-0.1 < \dot{x}_{1,a} < 0.1) \text{ \& } (0 < \dot{x}_{2,a} < 0.4).$$

Shell 1 is stationary and shell 2 has a smaller velocity than the precollision velocity of shell 1.

Stationary shell 1 (larger  $\dot{x}_{i,2}$ ):

$$(-0.1 < \dot{x}_{1,a} < 0.1) \text{ \& } (\dot{x}_{i,2} > 0.6).$$

Shell 1 is stationary and shell 2 has a larger velocity than the precollision velocity of shell 1.

Elastic collision of identical spheres:

$$(-0.1 < \dot{x}_{i,1} < 0.1) \text{ \& } (0.4 \leq \dot{x}_{2,a} \leq 0.6).$$

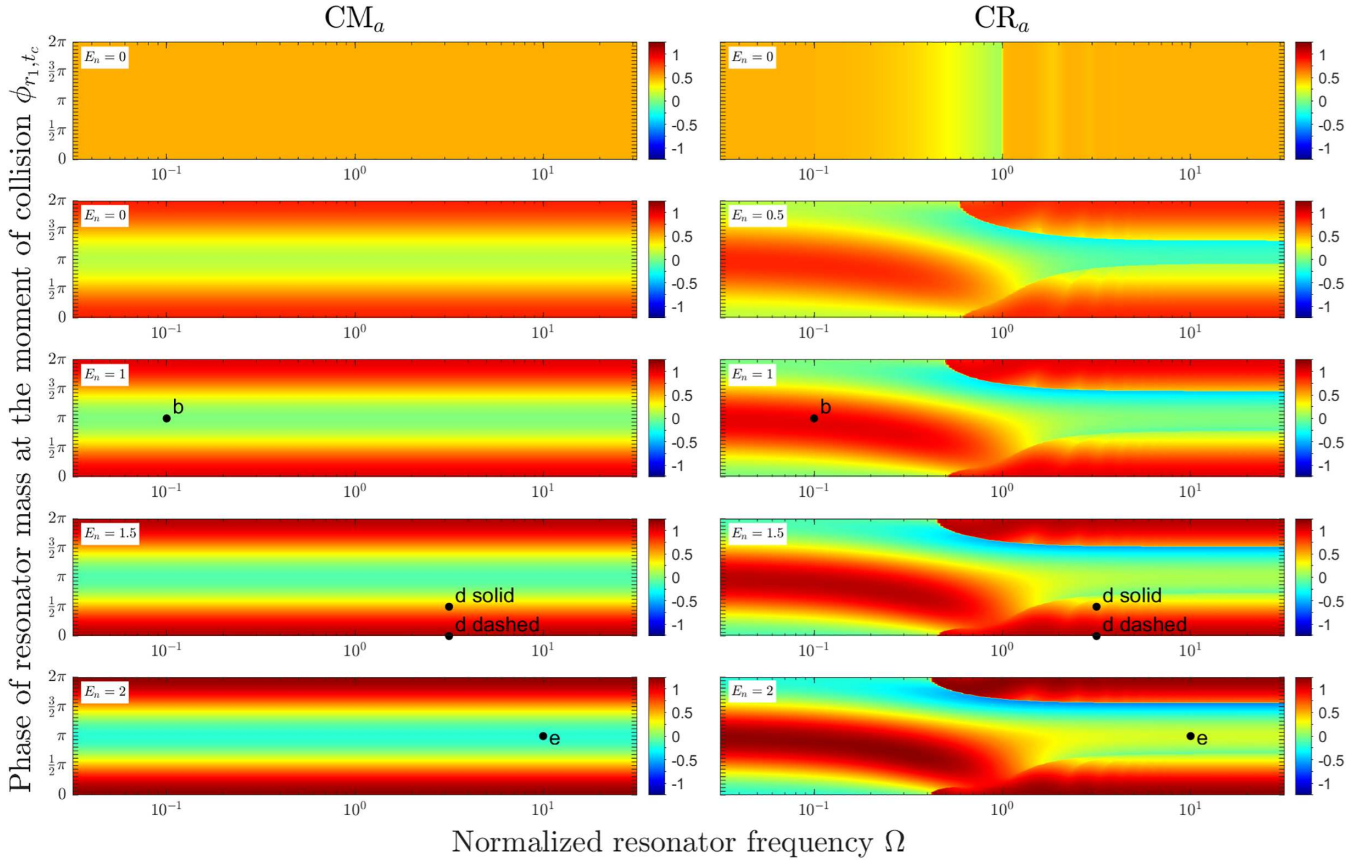


FIG. 2. Density plots for the effective coefficients of motion,  $CM_a$  (left panels), and restitution,  $CR_a$  (right panels), for the two mass-in-mass systems. The vertical axes represent the phase  $\phi_{r_1,tc}$  of resonator 1 at the moment of collision, and the horizontal axes represent the normalized frequency ratio  $\Omega$ . Each plot represents the results for different initial conditions of the left-hand mass-in-mass system at the moment of collision. The order from top to bottom in each case corresponds to increasing total energy of the resonator. The labeled data points correspond to selected parameters, as shown in the panels of Fig. 5.

Shell 1 is stationary and shell 2 has the precollision velocity of shell 1.

The white regions represent nonphysical solutions. Region boundaries incorporate tolerances ensuring clear visibility. For practical characterization, some regions require specific velocity ratios, whereas others use fixed velocity bounds.

Figure 2 shows that when  $\Omega < 1$ , the variations of  $CR_a$  and  $CM_a$  with resonator phase exhibit an offset relative to each other (i.e., their peak positive and negative values occur at different resonator phases), whereas when  $\Omega > 1$ , their positive variations are phase-synchronized. Comparison with Fig. 3 reveals that the offset regime ( $\Omega < 1$ ) corresponds to dynamics where both shells acquire nonzero velocities, whereas the phase-synchronized regime ( $\Omega > 1$ ) yields cases where one shell remains stationary postcollision.

$CR_a$  in Eqs. (6) is directly equivalent to the conventional coefficient of restitution in Eqs. (5). In the conventional case, when there is no attractive force between the entities during the collision and no process that causes the particles to stick together, this coefficient represents how well kinetic energy is conserved during the collision. It ranges from 0 for a completely inelastic collision to 1 for a completely elastic collision. A value of 0 indicates that the final momentum is equally distributed, and the entities couple together, whereas

a value of 1 implies that all of the momentum is transferred to the second entity, provided they have equal mass.

The effective coefficient of motion  $CM_a$  in Eqs. (6) is equivalent to the fixed unity term in Eqs. (5), which in the conventional case of identical simple spheres results from the conservation of momentum. This new term therefore arises from the effective momentum conservation of the spherical shells.

The top panel in Fig. 2 represents the case in which no energy is stored in the resonator of the mass-in-mass system 1 at the moment of impact. As expected from Eqs. (14b),  $CM_a$  is fixed at 0.5, which is equivalent to the nonresonant case described earlier with  $m + m_r = 2m$ . This case also eliminates the effect of the resonator phase on the effective coefficient of restitution,  $CR_a$ . The effective coefficient of restitution remains a function of the resonator frequency, exhibiting a resonant-like effect with a dip to zero as the resonator frequency approaches the compression frequency from below. The asymptotic values correspond to the nonresonant case.

The top panel of Fig. 3 (zero resonator energy) shows the standard Newton's cradle response for elastic collisions (dark blue region) at the asymptotic limits, where both effective parameters match the nonresonant system. As  $\Omega$  decreases below 1 and  $CR_a$  approaches zero (while  $CM_a$  remains fixed at



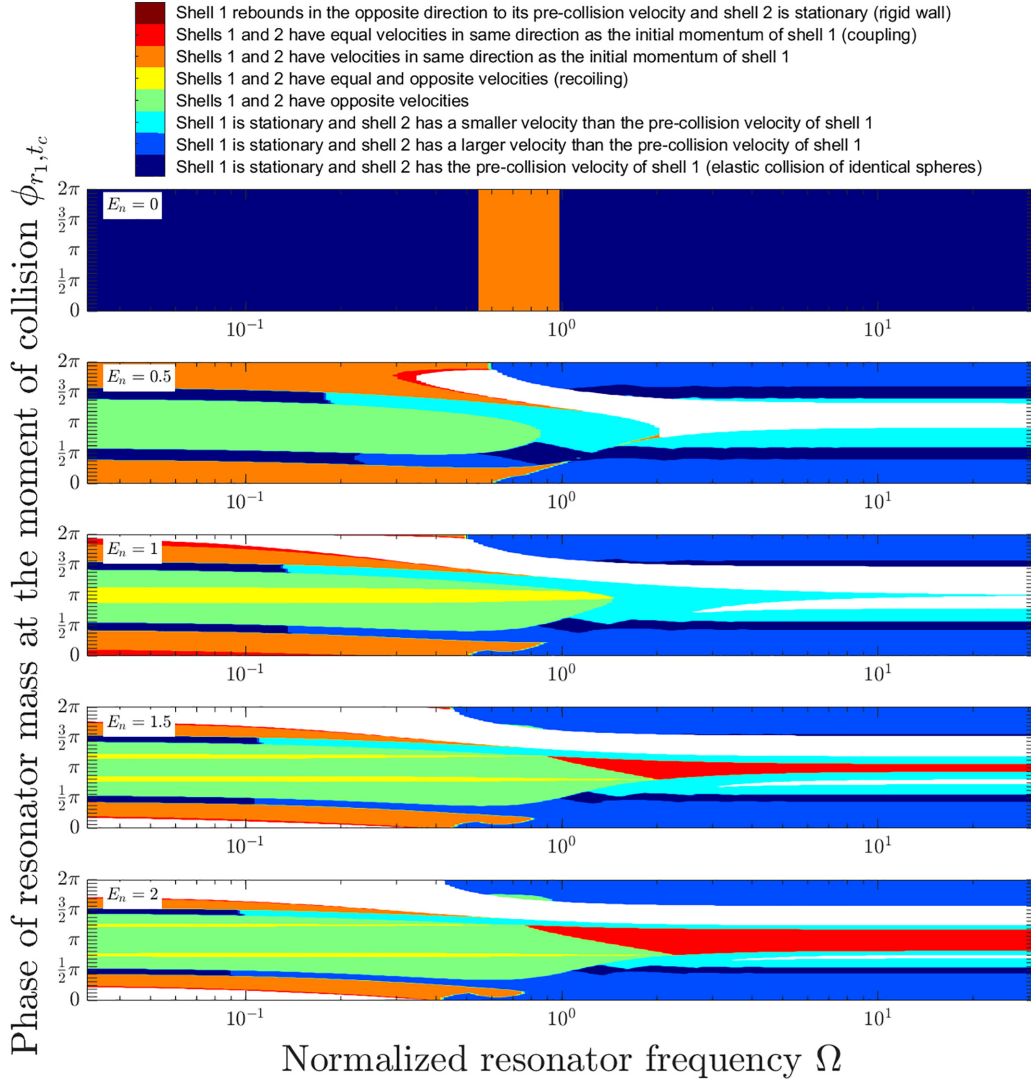


FIG. 3. Density plots representing a “phase diagram” of the possible responses (see text next to the color scale) characterizing the dynamics of the two colliding mass-in-mass systems. The vertical axes represent the phase  $\phi_{r_1, t_c}$  of the resonator 1 at the moment of collision, and the horizontal axes show the normalized frequency ratio  $\Omega$ . The order from top to bottom in each case corresponds to increasing total energy of the resonator. The labeled data points correspond to selected parameters, as shown in the panels of Fig. 5.

0.5), the collision becomes inelastic (orange region), causing both shells to move together in the direction of shell 1’s initial momentum.

By introducing initial conditions with nonzero resonator energy of the mass-in-mass system 1, a much larger range and combination of effective coefficients can be achieved. For both effective parameters, the sign of the resonator’s velocity at the moment of collision has the strongest effect on the relative change of their values.

Unlike in the conventional case,  $CM_a$  can vary since the outer spherical shells on their own are not a closed system, i.e.,  $CM_a$  is governed by the total momentum of the spherical shells postcollision relative to the value of the momentum precollision. Figure 2 and Eqs. (14b) show that  $CM_a$  is not a function of the resonator frequency  $\omega_r$ , but rather is simply determined by the velocity of the resonant inner mass at the moment of collision. A positive value is associated with an effective addition of momentum to the system of spherical shells. In contrast, a negative value is associated with a re-

duction in the momentum of the system of spherical shells; when  $\dot{x}_{r, t_c} < -\dot{x}_{1, t_c}$ ,  $CM_a$  becomes negative, meaning the momentum of the system of spherical shells is directed opposite to its initial direction.

The yellow regions in Fig. 3 indicate recoil dynamics where the shells move with equal but opposite velocities (zero net momentum), corresponding to  $CM_a = 0$  in Fig. 2. The dark red regions show rigid-wall-like behavior: Shell 1 rebounds opposite to its initial velocity while shell 2 remains stationary. For identical shells, this requires  $CM_a = -1$  and  $CR_a = 1$ , as confirmed by the values in Fig. 2.

Figure 2 shows that the effective coefficient of restitution  $CR_a$  can exceed 1, indicating that kinetic energy is being added to the spherical shells. The source of this kinetic energy is the energy stored in the resonator of mass-in-mass system 1 at the moment of collision. For resonator frequencies below the compression frequency during contact (i.e.,  $\Omega < 1$ ),  $CR_a$  tends to increase when the resonator’s phase is  $\pi$  (negative resonator velocity) and decrease when the phase is 0 or  $2\pi$

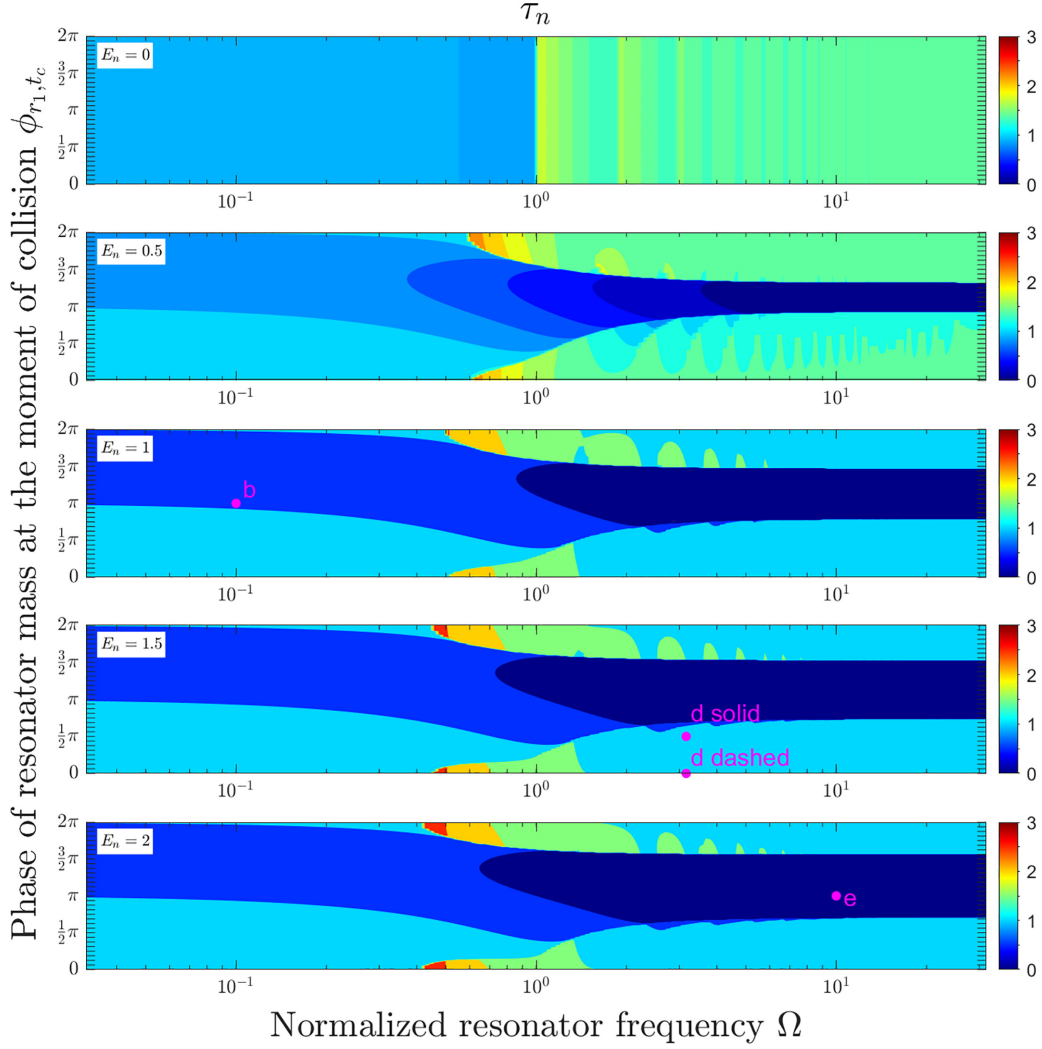


FIG. 4. Density plots of the contact duration  $\tau_n$  of the two colliding mass-in-mass systems, normalized to the contact duration for an equivalent shell containing no internal mass. The vertical axes represent the phase  $\phi_{r_1, t_c}$  of resonator 1 at the moment of collision, and the horizontal axes show the normalized frequency ratio  $\Omega$ . The order from top to bottom in each case corresponds to increasing total energy of the resonator. The labeled data points correspond to selected parameters, as shown in the panels of Fig. 5.

(positive resonator velocity). This trend reverses for resonator frequencies above the compression frequency (i.e.,  $\Omega > 1$ ).

For  $\Omega > 1$ , the midblue regions in Fig. 3 exhibit dynamics identical to collisions between nonresonant shells (i.e., shell 1 becomes stationary after collision). However, since both  $CR_a > 1$  and  $CM_a > 1$  with  $CR_a \approx CM_a$  in these regions, shell 2 moves faster than shell 1's precollision velocity.

The green regions in the right-hand panels of Fig. 2 correspond to  $CR_a \approx 0$ . As expected for a completely inelastic collision, Fig. 3 confirms that the shells couple together (red regions) and move with nearly identical velocities after separation.

Figure 2 also shows that the coefficient of restitution  $CR_a$  can take negative values. However, these regions mostly correlate with the white regions associated with nonphysical solutions in Fig. 3. Unless the average displacement of mass-in-mass system 2 in the external potential is equal to or greater than the (positive) displacement of system 1 after impact, the entities will collide again shortly after the initial collision. The exact timing of this subsequent collision depends on the

phase of the resonant oscillatory motion superimposed on the motion in the general external potential. As indicated by Eqs. (11) and (13), negative values of  $CR_a$  will quickly lead to fragmentation of the general oscillatory behavior in the external potential.

Figure 4 shows density plots of the normalized contact duration (color scale) for the two colliding mass-in-mass systems, determined through numerical simulations of collisions governed by Eqs. (1). The dominant effect is contact-time reduction when  $\Omega > 1$  and resonator velocity is negative [ $\phi_{r_1, t_c} \in (\pi/2, 3\pi/2)$ ]. In this case, the resonator motion creates negative relative displacement ( $x_{r_1} - x_1 < 0$ ), generating a leftward force on shell 1. This effect is most pronounced near  $\phi = \pi$  where the maximum leftward velocity occurs. The contact duration remains relatively unchanged for  $\Omega < 0.1$ , as the slower internal mass oscillation cannot release or absorb much energy, and thus has a much smaller effect on the compression time.

The strongest prolonging effect occurs when  $\phi_{r_1, t_c} \approx 0$  or  $2\pi$ , corresponding to positive resonator velocity at

impact. As the resonator moves rightward, positive relative displacement develops ( $x_{r1} - x_1 > 0$ ), generating an increasing rightward force on shell 1 that maintains contact. When the resonator frequency is just below the compression frequency ( $\Omega \approx 0.4$  to 1), the relative displacement evolves slowly, sustaining the rightward force throughout the contact period and prolonging the collision.

### B. Simulated dynamics of a particular system

We selected parameter combinations expected to yield nonconventional postcollision dynamics. We now present the resulting real-time behavior, highlighting the most striking visual effects. To illustrate how different effective coefficients influence postcollision motion, the left-hand panels, Figs. 5(a)–5(e), show simulated shell trajectories over six successive collisions in an external gravitational potential. Time is plotted on the vertical axis, increasing downward from zero, enabling observation of horizontal shell displacements over time. The right-hand panels, Figs. 5(f)–5(i), depict outer-shell and internal-mass motion during the first collision, corresponding to the dynamics shown in the respective left-hand panels. Since actual collision displacements are much smaller than the dimensions of the masses, displacements in these panels are scaled by the indicated factors for visualization. These results demonstrate that even minuscule internal-mass displacements—typically three orders of magnitude smaller than shell displacements—can significantly influence postcollision motion. Displacements are obtained from numerical simulations (MathWorks Simulink) of the full equations of motion, incorporating both collision dynamics [Eqs. (1)] and external-potential oscillations [Eqs. (2)], for representative parameter combinations. Animations of each scenario are available in the Supplemental Material [19]. Figure 5(a) represents the conventional case of two simple spheres, each with mass  $m$ .

Figure 5(b) illustrates the response of the outer spherical shells for a chosen normalized resonator frequency  $\Omega = 0.1$ , phase  $\phi = \pi$  and normalized initial energy  $E_n = 1$ , corresponding to  $CM_a = 0$  and  $CR_a = 0.98$ . The condition  $CM_a = 0$  implies zero net momentum for the spherical shells after collision, causing them to recoil with equal and opposite velocities. The coefficient  $CR_a$  governs their relative velocity magnitude, with  $CR_a = 0.98$  indicating a nearly elastic collision where each shell's postimpact speed is approximately half of shell 1's precollision velocity.

The peak displacements in the external potential are roughly equal and opposite due to the symmetric velocity distribution. In conventional sphere collisions, such opposite velocities require unequal masses. While these effective parameters apply specifically to the first collision, subsequent collisions exhibit similar oscillatory patterns.

Figure 5(f) reveals that at the end of the first collision, the internal mass of shell 1 moves leftward due to its initial negative velocity ( $\phi = \pi$ ), pulling shell 1 backward against its initial trajectory. Meanwhile, the internal mass of shell 2 remains nearly stationary, resulting in conventional postcollision motion for shell 2, albeit with reduced velocity due to energy retention in shell 1.

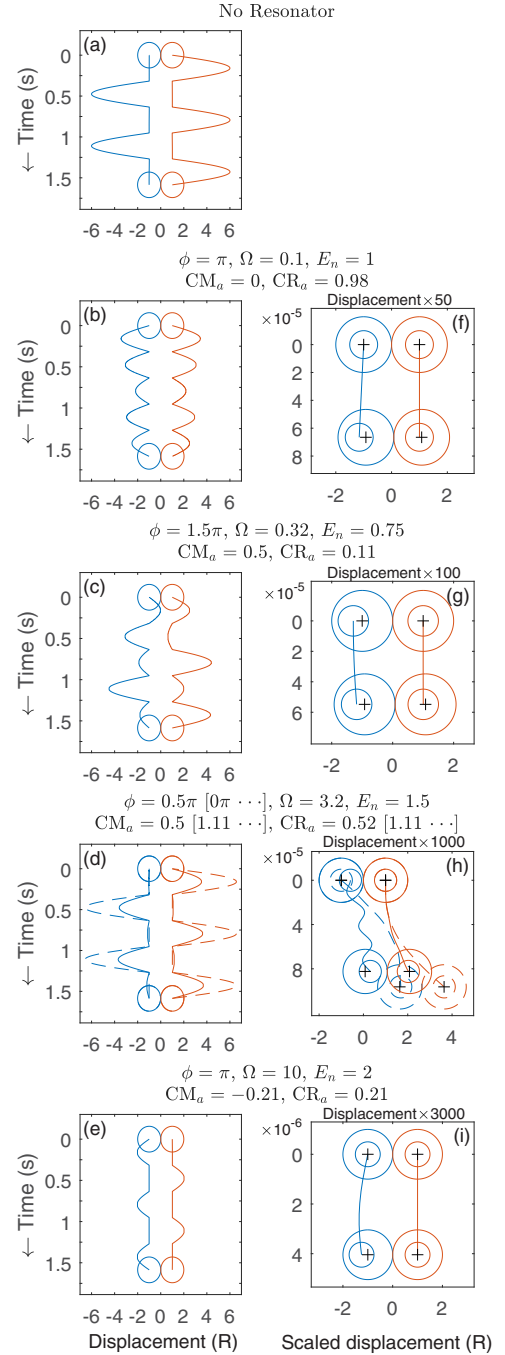


FIG. 5. Time-domain displacement plots showing the motion of the two spherical shells for selected resonator parameters and initial conditions corresponding to a range of values of the effective coefficients of motion,  $CM_a$ , and restitution,  $CR_a$ . Shell 2 and its resonator are initially stationary at the equilibrium point (with zero kinetic and potential energy) at the time of collision (time = 0 s). The left-hand panels (a)–(e) show the motion of the outer shells over the first six collisions. Panel (a) shows the time response for conventional solid spheres (no resonators), whereas panels (b)–(e) show the time response for different parameters and initial conditions, as indicated in each panel. The right-hand panels (f)–(i) display the displacement of both the outer and inner shells (scaled as indicated above each panel) during the initial collision for each sequence shown in the corresponding left panel. The black crosses indicate the centers of each outer sphere at the start and end times.

Figure 5(c) shows the response for  $\Omega = 0.32$ ,  $\phi = 1.5\pi$ , and  $E_n = 0.75$ , yielding  $CM_a = 0.5$  and  $CR_a = 0.11$ . Whereas  $CR_a = 0$  would indicate perfect inelastic coupling, the chosen  $CR_a = 0.11$  prevents immediate recollision by allowing slight separation. The value  $CM_a = 0.5$  indicates the shells retain half the initial momentum, resulting in reduced oscillation amplitudes compared to conventional collisions.

Figure 5(g) shows that the initial negative displacement of shell 1's internal mass creates immediate leftward force on its shell. As the resonator moves rightward during spring decompression, the leftward force weakens but remains negative throughout contact. Shell 2's internal mass remains nearly stationary, resulting in reduced momentum transfer similar to Figs. 5(b) and 5(f).

Figure 5(d) shows the response for  $\Omega = 3.2$  and  $E_n = 1.5$  at two phases:  $\phi = 0$  (dashed line,  $CM_a = CR_a = 1.1$ ) and  $\phi = 0.5\pi$  (solid line,  $CM_a = CR_a = 0.5$ ). Both cases show shell 1 stationary postcollision (conventional elastic behavior), but shell 2's displacement magnitude increases by 10% for  $\phi = 0$  and decreases by 50% for  $\phi = 0.5\pi$  relative to conventional cases. Such momentum scaling would conventionally require unequal masses and energy gain or loss in the collision.

Figure 5(h) shows enhanced shell displacements during collision due to  $\Omega > 1$  and prolonged contact. For  $\phi = 0$  (dashed line), the internal mass's positive momentum partially transfers to shell 2, amplifying its displacement. For  $\phi = 0.5\pi$  (solid line), the internal mass's initial rightward displacement and subsequent leftward motion reduce net momentum transfer.

Figure 5(e) shows the response for  $\Omega = 10$ ,  $\phi = \pi$ , and  $E_n = 2$ , producing  $CM_a < 0$ . When  $CR_a \approx -CM_a$ , the dynamics resemble a sphere colliding with a rigid wall: Shell 1 rebounds while shell 2 remains stationary. This occurs when net momentum transfer to shell 2 is negligible and shell 1's internal resonator provides sufficient recoil momentum via negative velocity at  $\phi = \pi$ . Figure 5(i) confirms the reduced contact time limits momentum transfer to shell 2.

#### IV. CONCLUSIONS

In conclusion, we have analyzed the collision dynamics of a meta-atom based two-sphere Newton's cradle system and derived theoretical expressions for the effective coefficients of restitution and motion. The analysis focused on the case in which the local resonance can be considered strong, that is, where it has a much higher resonant frequency than the independent oscillations of the two mass-in-mass systems in the external gravitational potential.

We show that using a two-sphere mass-in-mass system in a Newton's cradle geometry results in more complex behavior than in the conventional case, depending on the initial conditions of the internal resonator mass at the moment of collision. Our results demonstrate that the effective coefficient of motion can be negative, causing the momentum of the outer spherical shells to be reversed by the resonant behavior of the inner-mass. The effective coefficient of restitution exhibits a range of values, providing a much richer spectrum of dynamic behavior compared to the conventional two-sphere Newton's cradle. We also show that, in general, the magnitude ranges of both effective parameters increase with increasing resonator energy, whereas the contact duration of the shells decreases with increasing resonator energy. The sign of the resonator velocity at the moment of collision is shown to have a significant effect on the subsequent dynamics.

Our derived effective parameters suggest the existence of exotic properties in both extended arrays of colliding mass-in-mass units and equivalent periodic lattices composed of mass-in-mass unit cells, which may have practical applications. Generalizing these results will be the focus of future work. Periodic lattices could include granular materials with alternating compressed and uncompressed regions that exhibit collisions between adjacent units, as well as lattices composed of units connected by fixed links but spaced closely enough to allow collisions.

Our findings are particularly relevant to the design of effective dynamical parameters in metamaterials based on locally resonant behavior, as they demonstrate how effective momentum and energy conservation can be tuned via the initial conditions of local resonators. Further work is needed to extend these results to scenarios involving larger-amplitude oscillations and frictional effects. Ultimately, this line of research may enable the construction and exploration of new classes of "collision" metamaterial structures.

#### ACKNOWLEDGMENTS

S.A.P. was supported by the UK Engineering and Physical Sciences Research Council through Grant No. EP/T028661/1. O.B.W. acknowledges Grants-in-Aid for Scientific Research from the Ministry of Education, Culture, Sports, Science and Technology (MEXT).

#### DATA AVAILABILITY

The data that support the findings of this article are openly available [25], embargo periods may apply.

- 
- [1] Y. Liu and X. Zhang, Metamaterials: A new frontier of science and technology, *Chem. Soc. Rev.* **40**, 2494 (2011).
  - [2] A. Banerjee, R. Das, and E. P. Calius, Waves in structured mediums or metamaterials: A review, *Arch. Comput. Methods Eng.* **26**, 1029 (2019).
  - [3] G. W. Milton, M. Briane, and J. R. Willis, On cloaking for elasticity and physical equations with a transformation invariant form, *New J. Phys.* **8**, 248 (2006).
  - [4] S. Guenneau, A. Movchan, G. Pétursson, and S. Anantha Ramakrishna, Acoustic metamaterials for sound focusing and confinement, *New J. Phys.* **9**, 399 (2007).
  - [5] H. Huang, C. Sun, and G. Huang, On the negative effective mass density in acoustic metamaterials, *Int. J. Eng. Sci.* **47**, 610 (2009).
  - [6] S. H. Lee and O. B. Wright, Origin of negative density and modulus in acoustic metamaterials, *Phys. Rev. B* **93**, 024302 (2016).



- [7] E. Kim and J. Yang, Review: Wave propagation in granular metamaterials, *Funct. Compos. Struct.* **1**, 012002 (2019).
- [8] G. Gantzounis, M. Serra-Garcia, K. Homma, J. M. Mendoza, and C. Daraio, Granular metamaterials for vibration mitigation, *J. Appl. Phys.* **114**, 093514 (2013).
- [9] P. G. Kevrekidis, A. Vainchtein, M. S. Garcia, and C. Daraio, Interaction of traveling waves with mass-with-mass defects within a Hertzian chain, *Phys. Rev. E* **87**, 042911 (2013).
- [10] F. Hadadifard and J. D. Wright, Mass-in-mass lattices with small internal resonators, *Stud. Appl. Math.* **146**, 81 (2021).
- [11] H. Xu, P. G. Kevrekidis, and A. Stefanov, Traveling waves and their tails in locally resonant granular systems, *J. Phys. A: Math. Theor.* **48**, 195204 (2015).
- [12] P. G. Kevrekidis, A. G. Stefanov, and H. Xu, Traveling waves for the mass in mass model of granular chains, *Lett. Math. Phys.* **106**, 1067 (2016).
- [13] L. Liu, G. James, P. Kevrekidis, and A. Vainchtein, Breathers in a locally resonant granular chain with precompression, *Physica D* **331**, 27 (2016).
- [14] L. Liu, G. James, P. Kevrekidis, and A. Vainchtein, Strongly nonlinear waves in locally resonant granular chains, *Nonlinearity* **29**, 3496 (2016).
- [15] L. Bonanomi, G. Theocharis, and C. Daraio, Wave propagation in granular chains with local resonances, *Phys. Rev. E* **91**, 033208 (2015).
- [16] E. Kim, J. Yang, H. Hwang, and C. W. Shul, Impact and blast mitigation using locally resonant woodpile metamaterials, *Int. J. Impact Eng.* **101**, 24 (2017).
- [17] C. M. Donahue, C. M. Hrenya, R. H. Davis, K. J. Nakagawa, A. P. Zelinskaya, and G. G. Joseph, Stokes' cradle: Normal three-body collisions between wetted particles, *J. Fluid Mech.* **650**, 479 (2010).
- [18] C. M. Donahue, C. M. Hrenya, and R. H. Davis, Stokes's cradle: Newton's cradle with liquid coating, *Phys. Rev. Lett.* **105**, 034501 (2010).
- [19] See Supplemental Material at <http://link.aps.org/supplemental/10.1103/2whk-jc4b> for the derivation of the pendulum dynamics of the two-sphere mass-in-mass Newton's cradle; derivation of the instantaneous effective coefficients of restitution  $CR_e$  and motion  $CM_e$ ; derivation of the postcollision velocity in the external potential; derivation of the overall effective coefficient of restitution  $CR_o$  and effective coefficient of motion  $CM_o$  for the average postcollision motion; density plots for the initial velocities of each spherical shell in the external potential after impact; and the animations of the simulated motion of the dynamics of the system for several different values of the resonator parameters and precollision energy.
- [20] S. Hutzler, G. Delaney, D. Weaire, and F. MacLeod, Rocking Newton's cradle, *Am. J. Phys.* **72**, 1508 (2004).
- [21] H. Hertz, On the contact of elastic solids, *Z. Reine Angew. Mathematik* **92**, 156 (1881).
- [22] L. Landau and E. Lifshitz, *Theory of Elasticity*, 3rd ed., Course of Theoretical Physics (Butterworth-Heinemann, Oxford, UK, 1986).
- [23] F. Herrmann and M. Seitz, How does the ball-chain work? *Am. J. Phys.* **50**, 977 (1982).
- [24] K. L. Johnson, *Contact Mechanics* (Cambridge University Press, Cambridge, UK, 1987).
- [25] <https://github.com/sapope-cmyk/Meta-atom-collisions>.

*Correction:* A typographical error in the first sentence of the abstract has been fixed.